CFD model for tubular SOFC stack fed directly by biomass

International Journal of Hydrogen Energy

CFD model for tubular SOFC stack fed directly by biomass

--Manuscript Draft--

Manuscript Number:	
Article Type:	Short Communication
Section/Category:	Fuel Cells & Applications
Keywords:	Electrochemistry; SOFC Stack; Biomass; Gasification; COMSOL Multiphysics®; DB-SOFC
Corresponding Author:	DAVIDE PAPURELLO, Ph.D. Politecnico di Torino turin, ITALY
First Author:	DAVIDE PAPURELLO, Ph.D.
Order of Authors:	DAVIDE PAPURELLO, Ph.D.
	Davide Canuto
	Massimo Santarelli
Abstract:	The energy transition can also benefit from the exploitation of biomass. Residual biomass in Mediterranean areas can be exploited to a greater extent through highly efficient fuel cell systems. The Direct Biomass-SOFC project is based on a direct coupling between biomass power supply and SOFC tubular cells. This research project stems from the need to cover the growing need for electricity by avoiding the use of non-renewable sources, with unused or little-used sources that can be exploited from the Mediterranean area. To this purpose, analyses were conducted to model a SOFC tubular cell stack by investigating the optimal configuration. The basic objective is to dimension a SOFC tubular cell stack, fed by syngas to produce at least 200 W. Two configurations were chosen: a square and a circular arrangement. Another objective of the study is to choose the best temperature control system. A pressurised water system and an air system are studied. The results show that the best performance is guaranteed by a square arrangement with an air temperature control system. The maximum electrical power produced is 225 W.

Politecnico di Torino

Energy Center, Via Borsellino 38/18 – Turin (ITA)
Dipartimento di Energia – Fuel Cell and Hydrogen Technologies Group
Energy Center Lab. Group

Davide Papurello, Ph.D.

Dipartimento di Energia - Politecnico di Torino

Energy Center, Politecnico di Torino, Via Paolo Borsellino 38/18, 10138 Turin, Italy

E-mail: davide.papurello@polito.it

Phone: +39.011.090.4514 / 011.090.8505

Mobile +39.340.2351692

To the Editors of International Journal of Hydrogen Energy

OBJECT: Submission of the article manuscript entitled *"CFD model for tubular SOFC stack fed directly by biomass"*

Dear Editor(s),

We are submitting to your kind attention a work focused on The energy transition can also benefit from the exploitation of biomass. Residual biomass in Mediterranean areas can be exploited to a greater extent through highly efficient fuel cell systems. The Direct Biomass-SOFC project is based on a direct coupling between biomass power supply and SOFC tubular cells. This research project stems from the need to cover the growing need for electricity by avoiding the use of non-renewable sources, with unused or little-used sources that can be exploited from the Mediterranean area.

All authors agree for submitting the manuscript.

The manuscript is original work of authors and has not been submitted earlier.

Politecnico di Torino

Energy Center, Via Borsellino 38/18 – Turin (ITA)
Dipartimento di Energia – Fuel Cell and Hydrogen Technologies Group
Energy Center Lab. Group

I am available as a reviewer.

Thank you for your kind attention.

Best Regards,

Torino | August 13, 2021

Davide Papurello

On behalf of all Authors

Dipartimento Energia | Department of Energy
Politecnico di Torino Corso Duca degli Abruzzi, 24 – 10129 Torino – Italia
tel: +39 011.090.4514 /8505
davide.papurello@polito.it www.denerg.polito.it www.polito.it

Highlights

- The Direct Biomass SOFC system was developed numerically for 25 tubolar cells
- 25 tubolar cells were able to produce 225 W from syngas
- The square tubolar cell arrangement showed better results
- The air temperature control system showed better results

CFD model for tubular SOFC stack fed directly by biomass

Davide Papurello[*], *Davide Canuto*, *Massimo Santarelli*

Department of Energy (DENERG), Politecnico di Torino, Corso Duca degli Abruzzi, 24, 10129, Turin, Italy.

*Corresponding author. Tel.:+393402351692. *Email address*: davide.papurello@polito.it

Abstract

The energy transition can also benefit from the exploitation of biomass. Residual biomass in Mediterranean areas can be exploited to a greater extent through highly efficient fuel cell systems. The Direct Biomass-SOFC project is based on a direct coupling between biomass power supply and SOFC tubular cells. This research project stems from the need to cover the growing need for electricity by avoiding the use of non-renewable sources, with unused or little-used sources that can be exploited from the Mediterranean area.

To this purpose, analyses were conducted to model a SOFC tubular cell stack by investigating the optimal configuration. The basic objective is to dimension a SOFC tubular cell stack, fed by syngas to produce at least 200 W. Two configurations were chosen: a square and a circular arrangement. Another objective of the study is to choose the best temperature control system. A pressurised water system and an air system are studied. The results show that the best performance is guaranteed by a square arrangement with an air temperature control system. The maximum electrical power produced is 225 W.

Nomenclature

$A_{i,an/cat}$	Pre-exponential factor [S/m^2]
AU	Air Utilization [-]
c_p	gas specific heat capacity [J/(kgK)]
CFD	Computational Fluid Dynamic
CHP	Combined Heat and Power
d_{pore}	diameter of electrodes pore [m]
D_{eq}	equivalent diameter [m]
D^{eff}	Effective diffusion coefficient [m^2/s]
$D_i^{F,K}$	sum of Fick and Knudsen diffusion coefficient [m^2/s]
D_i^K	Knudsen diffusion coefficient of a generic species *i* [m^2/s]
D_{ij}	Binary diffusion coefficient [m^2/s]
E	Equilibrium potential [V]
$E_{act,an/cat}$	Activation Energy [J/mol]
F	Faraday's constant [C/mol]
FU	Fuel Utilization [-]
H	Heat of reaction [J/mol]
h	Convective heat transfer coefficient [W/m^{2}K]
$\bar{h}$	molar enthalpy [J/mol]
i	current density [A/cm^2]
$i_{0,\,an/cat}$	equilibrium current density [A/cm^2]
i_l	limiting current density [A/cm^2]
K_{pr}	SMR Equilibrium constant [Pa]
K_{ps}	WGS Equilibrium constant [-]
k	thermal conductivity [W/(m*K)]
$k_{r,forward/backward}$	SMR catalysed reaction rate constant [-]
$k_{s,forward/backward}$	WGS catalysed reaction rate constant [-]
LSM	Lanthanum Strotium Manganite
Ni/YSZ	Yttria Stabilized Zirconia within atoms of metallic Nickel
M_i	Molar mass [kg/mol]
$\dot{n}$	Molar flow [mol/s]

OK	Olive Kernel
Pr	Prandtl number [-]
p	pressure [Pa]
p_0	ambient pressure [Pa]
Q	thermal source/sink [W/m^3]
Q	conductive heat flux [W/m^2]
Re	Reynolds number [-]
$R_{r/s}$	Volumetric rate of reaction [mol/(m^{3}s)]
$\bar{R}$	universal gas constant [J/molK]
$\bar{s}$	molar entropy [J/molK]
SDG	Sustainable Development Goal
SMR	Steam Methane Reforming
SOFC	Solid Oxide Fuel Cell
T	Temperature [K]
TPB	Three Phase Boundary
U	velocity vector [m/s]
x_i	molar fraction [-]
WGS	Water Gas Shift reaction
Z	charge number [-]

Greek symbols

δ	thickness of diffusion [m]
ε	porosity [-]
ρ	gas density [kg/m^3]
σ_i	mean characteristic length of species i [Å]
τ	tortuosity [-]
Ω_D	dimensionless diffusion collision [-]

keywords

Electrochemistry; SOFC Stack; Biomass; Gasification; COMSOL Multiphysics®; DB-SOFC.

1. Introduction

Distributed power production is a good solution for sustainable development goals (SDG). Gonzalez et al. (2020) showed the main barriers for the biomass gasification systems for small power generation [1]. The search for new solutions in sustainable power generation is crucial given the increasing focus on the green transition. The main barriers can be grouped into Penetration of technology, Lack of information and Regulation and policy [2–4]. The problem of barriers can be overcome with the help of government policies that could help also the local community. The Penetration of technology could be assessed with engineered systems for energy production using a circular approach exploiting biomass sources. Many studies have presented interesting results regarding the use of biomass systems for energy production [1,5–8].

In the Mediterranean area, there is a substantial availability of residual biomass that could be adopted for sustainable energy production [9,10]. The biomass availability from these residual materials has been quantified by Velazquez-Marti et al. (2011) [10,11]. The residual biomass from olive pruning was quantified with an average of 1.31 t ha^{-1} from the annual pruning [10]. The residual biomass produced from vineyards was quantified at 2.15 t ha^{-1}, while the presence of irrigation increases the yields by 42% [11].

Zabaniotu (2014) focused on the CHP energy production fed by agro biomass [12]. The integration between a gasifier section and a SOFC stack was investigated considering olive kernels as starting biomass. The overall efficiency achieved 60% value, while commercial turbines achieve an overall efficiency around 40% [12].

Syngas used in SOFC systems should not contain sulphur [7,13] and tar compounds must be properly controlled using catalytic systems [14–16]. Sulphur compounds bind irreversibly above a certain concentration (>2-5 ppmv) with the catalytic active sites, reducing the TPB and consequently, the performance of the individual cell [17–19]. The phenomenon of carbon deposit formation from the presence of carbon-based trace compounds is investigated in the literature [20,21]. The solution generally adopted to limit the carbon deposition on SOFCs is the fuel mixing with the proper reforming agents [22,23], while trace contaminants (sulfur-based) should be removed through

adsorption systems [24–27]. Aravind et al. (2012) studied how biomass systems for syngas production can be integrated with high-temperature cleaning systems for the removal of unwanted compounds for SOFC systems [28]. These aspects are extensively studied in literature when there is no studies for the direct biomass feeding systems. The literature gap that should be addressed concern the tubular configuration system fed by syngas produced from biomass residues. In this paper, preliminary results from the direct biomass to SOFC stack system are presented. The goal of the DB-SOFC project is to produce 200 W of electrical power exploiting residual biomass that can be found in the Mediterranean area. Residual biomasses are exploited for the production of electricity and heat "directly" from the biomass that gasifies into the system. In our previous work, a single tubular cell is directly fed by syngas and it was modelled with encouraging results [29]. In this work, 25 tubular cells are directly fed by biomass derived from olive kernels. This biomass source needs to be treated in temperature. In this study, two different operating studies were selected before the injection into the stack (500 °C and 800 °C). Two different arrangements of the tubular cells and the cooling system were analysed. The cells were arranged in circular and in square configurations, while the cooling system was designed with pressurised liquid water and air.

2. Technology overview

25 tubular SOFC cells are placed vertically (Figure 1) and fed directly from the syngas produced from the biomass loaded in the upper part, with the help of the distribution screw. The anode side is directly exposed to the syngas, while air is injected into the cathode compartment via nozzles.

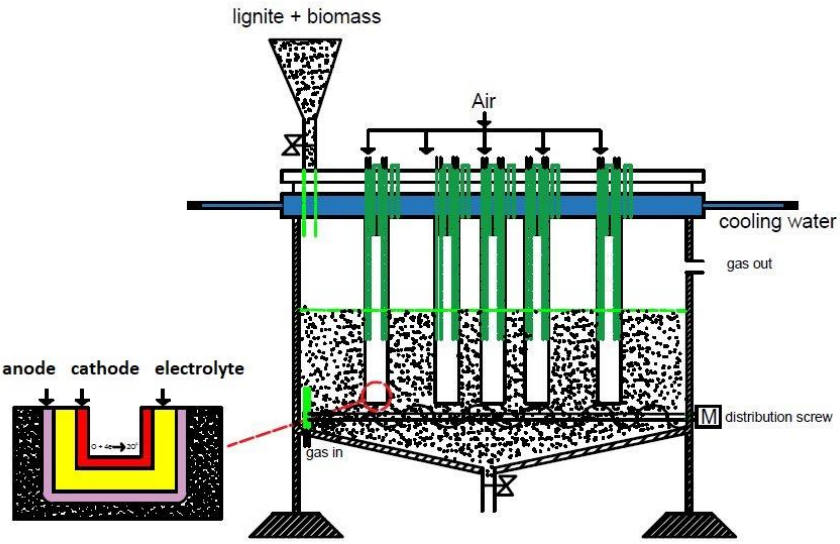

Figure 1. Vertical section of the stack

SOFCs are devices able to generate electrical power exploiting the syngas produced from the residual biomasses. The electrochemical reactions involved in the process are:

Anode)

$$H_2 + O^{2-} \rightarrow H_2O + 2e^- \quad (1)$$

$$CO + O^{2-} \rightarrow CO_2 + 2e^- \quad (2)$$

Cathode)

$$\frac{1}{2}O_2 + 2e^- \rightarrow O^{2-} \quad (3)$$

These reactions occur at the three-phase boundary, where oxygen ions, fuel molecules and electrons are involved in the process [30].

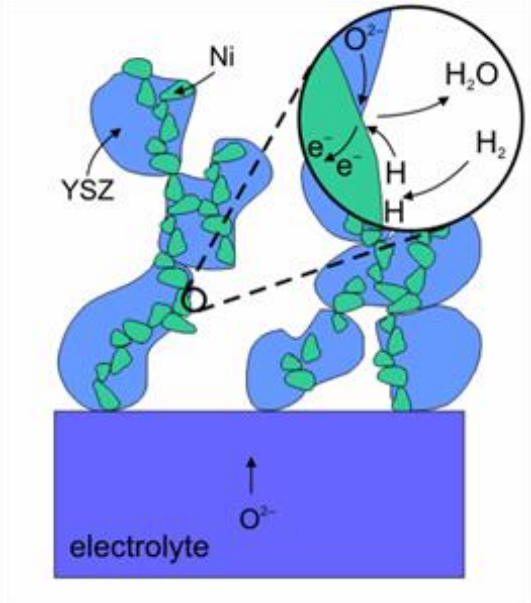

Figure 2. Anodic three-phase boundary [31]

The biomass is injected into the stack after a pre-treating process conducted at two different temperatures 500 and 800 °C for the performance investigation. The gasification process is conducted with CO_2, and/or H_2O, for the production of a gas mixture of H_2, H_2O, CO, CO_2 and CH_4. This mixture can feed the stack obtaining electrical and thermal energy. In addition, on the anodic side, two other reactions occur from the contact between methane and carbon monoxide with water vapour. They are the steam methane reforming (SMR) and the water gas shift (WGS):

SMR) $$CH_4 + H_2O \rightarrow 3H_2 + CO \qquad \Delta\bar{} = 206 \text{ KJ/mol} \qquad (4)$$

WGS) $$CO + H_2O \rightarrow H_2 + CO_2 \qquad \Delta\bar{} = -41.2 \text{ KJ/mol} \qquad (5)$$

There is also a screw biomass distributor within the system. This is a worm screw that is required to evenly distribute the pre-treated biomass pellets. In the upper part of the system, there is a water or air cooling system.

3. Material and methods

The tubular cells are made with conventional materials shown in the literature [20,32–34]. More in detail, the anode (thickness of 30 μm) is composed by the Cermet, a particular alloy composed by a ceramic matrix of Yttria Stabilized Zirconia within atoms of metallic Nickel (Ni/YSZ), the cathode

(thickness of 30 μm) is composed by the Lanthanum Strontium Manganite (LSM). The total diameter of a singular tubular cell is 2 cm.

The relevant features of the three materials are reported in the table below and some of these are assumed to be temperature-dependent.

Anode – Ni-YSZ	
Density [g/cm^3]	6.4 [35]
Electrical conductivity [S/m]	$\sigma_{an} = \frac{95*10^6}{T} * \exp(-\frac{1150}{T})$ [36]
Ionic conductivity [S/m]	10^{-1}
Tortuosity	3 [37]
Porosity	0.3 [38]
Cathode – LSM	
Density [g/cm^3]	5 [36]
Electrical conductivity [S/m]	$\sigma_{cat} = \frac{42*10^6}{T} * \exp(-\frac{1200}{T})$ [36]
Ionic conductivity [S/m]	$6.3*10^{-2}$ [39]
Tortuosity	5 [38]
Porosity	0.335 [38]

Table 1. Properties of the electrodes

Electrolyte – YSZ	
Electrical conductivity [S/m]	$1.75*10^{-2}$ [40]
Ionic conductivity [S/m]	$3.34 * 10^4 * \exp(-\frac{10300}{T})$ [36]
Density [g/cm^3]	5.16 [41]

Table 2. Properties of the electrolyte

The assumptions underlying the model developed with Comsol Mutiphysics® are listed here:

- Steady-state conditions;
- Initial temperature of a single cell sets to 800 °C;
- Nominal voltage sets to 0.7 V;

[1] I assume this quantity is the same of the electrolyte because the principal material is the same

- Dimensionless electrodes;
- No carbon deposition;
- Fast gasification process;
- Laminar flow of syngas and air in the flow channels;
- Velocity values of the inlet of air and syngas are, respectively, 0.4 m/s and 0.05 m/s [42]
- The reactant gas mixtures are approximated as an ideal gas;
- Three linear distributions of temperature were assumed for the inlet of the syngas.

Subsequently, it has been applied various physic nodes to the geometry to describe completely the phenomenon that will be presented in the detail.

Electrochemical model

This model is necessary to evaluate the voltage of every cell to estimate the current density of the stack, i [A*m^{-2}]. The current density is derived by the electrochemical reaction of H_2 and CO contained in the syngas mixture. The equilibrium potential equations on the anodic side are reported below [37,43]:

$$E_{H_2} = 1.253 - 0.00024516 * T + \frac{\bar{R}*T}{2*F} * ln\left[\frac{(p_{H_2})*(p_{O_2})^{0.5}}{(p_{H_2O})}\right] \quad (6)$$

$$E_{CO} = 1.46713 - 0.0004527 * T + \frac{\bar{R}*T}{2*F} * ln\left[\frac{(p_{CO})*(p_{O_2})^{0.5}}{(p_{CO_2})}\right] \quad (7)$$

in which the factor "2", before the Faraday's constant, represents the electrons exchanged in the oxidation reaction of H_2 and CO; p_i are the partial pressures of every i species involved in the reactions divided by the ambient pressure; T is the cell temperature and $\bar{R}$ is the universal gas constant.

For the evaluation of the activation overvoltages, it is used the Linearized Butler-Volmer equation with this anodic/cathodic transfer coefficient: ${\alpha_{an}}^{H_2} = 1.5$, ${\alpha_{cat}}^{H_2} = 0.5$, ${\alpha_{an}}^{CO} = 0.62$, ${\alpha_{cat}}^{CO} = 0.38$ and ${\alpha_{an/cat}}^{O_2} = 0.5$ [44]. Moreover, the activation current density for the anode and the cathode must be evaluated as reported in the article of Andersson et al. (2012) [41] and reported below:

$$i_{0,an} = \frac{\bar{R}*T}{Z_{an}*F} * A_{i,an} * exp\left(-\frac{E_{act,an}}{\bar{R}*T}\right) \quad (8)$$

$$i_{0,cat} = \frac{\bar{R}*T}{Z_{cat}*F} * A_{i,cat} * exp\left(-\frac{E_{act,cat}}{\bar{R}*T}\right) (9)$$

$A_{i,an/cat}$ are the pre-exponential factor and $E_{act,an/cat}$ are the activation energy of the two electrodes and their values are summarized in Table 5 [41]. As reported in Ni (2012) [37], the activation current density of the CO reaction at the anode has been supposed to be 40% of $i_{0,an}$.

$\mathbf{A_{i,an}}$ [S/m^2]	6.54*10^{11}
$\boldsymbol{A_{i,cat}}$ [S/m^2]	2.35*10^{11}
$\boldsymbol{E_{act,an}}$[J/mol]	1.4*10^5
$\boldsymbol{E_{act,cat}}$[J/mol]	1.37*10^5

Table 3. Values adopted for the evaluation of the equilibrium current densities

Diffusion model

The generation of diffusion overpotential in the cell, due to the motion of species involved in the flow channel and the porous electrodes, can be taken into account by evaluating the diffusion coefficients of the species involved in the process both at the anode and at the cathode. It is adopted the Fick's model, Ni (2013) [43]:

$$D_i^{eff} = \frac{\varepsilon}{\tau} * \left(\frac{1-x_i}{\sum_{j\neq i}\frac{x_j}{D_{ij}}} + D_i^K\right) \quad (10)$$

Where *x* is the molar fraction of the species considered and ε and τ are, respectively, the porosity and the tortuosity of the material. D_i^K, is the Knudsen diffusion coefficient for the porous electrodes according to Andersson et al. (2012) [41].

$$D_i^K = \frac{d_{pore}}{3} * \sqrt{\frac{8*\bar{R}*T}{\pi*M_i}} \quad (11)$$

with the pore diameter value (d_{pore}) is assumed to be 0.68 μm [41] and M_i is the molar mass of the species taken into account. The term D_{ij} (cm^2/s) is the binary diffusion coefficient [45]:

$$D_{ij} = \frac{0.0026*T^{1.5}}{p*\sqrt{\frac{2*M_i*M_j}{M_j+M_i}}*\left(\frac{\sigma_i+\sigma_j}{2}\right)^2*\Omega_D} \quad (12)$$

where p is the pressure (bar), of the total mixture containing the chemical species analyzed, $M_{i/j}$ are the molar mass in kg/mol and Ω_D is a dimensionless diffusion collision coefficient:

$$\Omega_D = \frac{1.06036}{B^{0.1561}} + \frac{0.193}{\exp(0.47635*B)} + \frac{1.03587}{\exp(1.52996*B)} + \frac{1.76474}{\exp(3.89411*B)} \quad (13)$$

$$B = \frac{k_b*T}{\sqrt{\varepsilon_i*\varepsilon_j}} \quad (14)$$

k_b is the Boltzmann's constant ($1.38066*10^{-23}$ J/K) and values of $\sigma_{i/j}$ and $\varepsilon_{i/j}$ are reported in Table 4.

	CO	CO_2	H_2	O_2	CH_4	N_2	H_2O
σ_i [Å]	3.69	3.941	2.827	3.467	3.758	3.798	2.641
ε_i/k_b [K]	91.7	195.2	59.7	106.7	148.6	71.4	809.1

Table 4. Values of εi/kb and σi [45]

Steam methane reforming and water gas shift reactions

Another fundamental modelization part is the methane reforming (SMR) and the CO shift reaction (WGS), which increase the hydrogen to carbon ratio inside the syngas mixture. The kinetic of these two reactions is shifted towards the products at a temperature of almost 800 °C for the SMR and at a temperature of almost 300 °C for the WGS.

It is assumed that the SMR occurs and it is favoured by the high temperature at which the SOFC works, whereas it cannot be the same for the WGS reaction. The equilibrium constant of both reactions is evaluated with the equations proposed by Haberman et al. (2004) [46] derived by experimental tests.

$$K_{pr} = 1.0267 * 10^{10} * \exp(-0.2513 * Z^4 + 0.3665 * Z^3 + 0.5810 * Z^2 - 27.134 * Z + 3.2770) \ [Pa] \quad (15)$$

$$K_{ps} = \exp(-0.2935 * Z^3 + 0.6351 * Z^2 + 4.1788 * Z + 0.3169) \quad (16)$$

in which

$$Z = \frac{1000}{T} - 1 \quad (17)$$

and, subsequently, the forward catalysed reaction rate constants are:

$$k_{r,forward} = 2395 * exp\left(-\frac{231266}{\bar{R}*T}\right); \quad (18)$$

$$k_{s,forward} = 0.0171 * exp\left(-\frac{103191}{\bar{R}*T}\right) \quad (19)$$

Finally, it is possible to obtain also the backward reaction rate thanks to the relation of the two catalysed reaction rate constants with the equilibrium constant.

$$K_{p,r/s} = \frac{k_{r/s,forward}}{k_{r/s,backward}} \quad (20)$$

Now, it is possible to estimate both the volumetric rate of reaction that is expressed in [mol m^{-3} s^{-1}], as follows [47].

$$R_r = k_{r,forward} * p_{CH_4} * p_{H_2O} - k_{r,backward} * p_{CO} * p_{H_2}^3 \quad (21)$$

$$R_s = k_{s,forward} * p_{CO} * p_{H_2O} - k_{s,backward} * p_{CO_2} * p_{H_2} \quad (22)$$

In conclusion, the molar rates of formation can be formulated and multiplied by the molar mass of the species taken into account, [kg*m^{-3}*s^{-1}].

$$\begin{cases} R_{CH_4} = -R_r * M_{CH_4} \\ R_{CO} = (R_r - R_s) * M_{CO} \\ R_{CO_2} = R_s * M_{CO_2} \\ R_{H_2O} = (-R_r - R_s) * M_{H_2O} \\ R_{H_2} = (3 * R_r + R_s) * M_{H_2} \end{cases} \quad (23)$$

Heat management

The heat transfer model is implemented on COMSOL® with the physic node *Heat transfer in Solids*.

$$\rho * c_p * u * \nabla T + \nabla q = Q \quad (24)$$

in which $\boldsymbol{u}$ is the velocity vector in m/s, ρ is the density of the gas in kg/m^3, c_p is the specific heat capacity of the gas [J/kg*K] and **Q** is the thermal source/sink in W/m^3. Furthermore, $\boldsymbol{q}$ is the conductive heat flux:

$$q = -k * \nabla T \quad (25)$$

The temperatures of the two fluids involved in the electrochemical process are inserted in the model as Dirichlet boundary conditions. The convective contribution is considered by introducing the

velocity field term in the cathodic and the anodic flow channels. Instead, for the heat generated, or absorbed, by the WGS and SMR is inserted a heat source boundary condition in which are summed the WGS heat generation contribution and the SMR endothermicity starting from:

$$\begin{cases} H_{SMR} = -(206205.5 + 19.51 * T) & \left[\frac{J}{mol}\right] \\ H_{WGS} = 45063 - 10.28 * T & \left[\frac{J}{mol}\right] \end{cases} \quad (26)$$

and multiplying each contribution with the respective rate of reaction R_r and R_s calculated in the previous paragraph [37,41].

In addition, the heat is generated due to other three contributions: heat generated by Joule heating in the cell, heat derived by the reaction irreversibilities that occur at the anode electrode and heat generated by the activation of the electrochemical reaction.

The heat generated by the irreversibilities is estimated by evaluating the entropy changes in the electrochemical reaction of hydrogen and carbon monoxide. These are evaluated from the Nist-Janaf thermochemical tables [48]. These values are reported in Table 5 for 800 °C.

$\bar{s}_{H2}$	$\bar{s}_{H2O}$	$\bar{s}_{CO}$	$\bar{s}_{CO2}$	$\bar{s}_{O2}$
166.83	236.06	236.34	274.15	245.83

Table 5. Molar entropies [kJ/molK] at 1073 K

The values of specific heat capacity and the conductivity of each material adopted are reported in Table 6.

Anode – Ni-YSZ	
Thermal conductivity, k_{AN} [W/mK]	11
Specific Heat, $c_{p,AN}$ [J/kgK]	450
Electrolyte – YSZ	
Thermal conductivity, k_{ELY} [W/mK]	2.7
Specific Heat, $c_{p,ELY}$ [J/kgK]	470
Cathode – LSM	

Thermal conductivity, k_{CAT} [W/mK]	6
Specific Heat, $c_{p,CAT}$ [J/kgK]	430

Table 6. Thermal parameters of every layer composing the cell [41]

The heat generated by the processes described above is controlled with a cooling system placed on top of the stack. In this work, it is designed in two ways: the first one with water at 200 °C and at a pressure of 18 bar, to avoid the evaporation of the fluid, and the second one with air at 650 °C.

The cooling system is modelled with the *Boundary Heat Source* in COMSOL®. The convective heat flux was built with the fluid temperature and the heat transfer coefficient. The heat transfer coefficient was calculated with the Dittus-Boelter correlation with the fluid circulating in a non-circular tube with an equivalent diameter of 0.03 m.

$$Nu = 0.023 * Re^{0.8} * Pr^{0.3} = \frac{h*D_{eq}}{k} \qquad (27)$$

$$Re = \frac{\rho*v*D_{eq}}{\mu} \; ; \qquad Pr = \frac{c_p*\mu}{k} \qquad (28)$$

The resulting heat transfer coefficients for the two cooling systems are 8370 $W*m^{-2}*K^{-1}$ for the water, and 161 $W*m^{-2}*K^{-1}$ for the air.

4. Results

Syngas gas mixture

The syngas molar concentration was achieved with the steam methane reforming and water gas shift reaction model, using the pre-treated biomass in two different conditions (500 and 800 °C). The starting biomass is the olive kernel (OK) with preliminary values already published (Table 7) [49].

Elemental analysis (wt%)	**Olive Kernel**
C	50.2
H	5.9

N	0.7
O	40.2
S	0.02
H/C	1.41
O/C	0.60

Table 7. Chemical analysis and heating values of raw samples

The production of the final products from the gasification model are: CO, CO_2, H_2, H_2O and CH_4. The scheme of the reactions is reported in our previous publication [29]. The results of the gasification model are shown in the following tables (Table 8 and 9) for the pre-treated biomass at 800 °C and 500 °C. The concentration distribution with the operating temperature within the system is shown in the supplementary material section.

	$x_{0,CH4}$	$x_{0,H2}$	$x_{0,CO}$	$x_{0,CO2}$	$x_{0,H2O}$
800 °C	$8.168*10^{-5}$	$9.72*10^{-3}$	$3.66*10^{-1}$	$4.41*10^{-1}$	$1.832*10^{-1}$
787.5 °C	$7.32*10^{-5}$	$8.13*10^{-3}$	$3.25*10^{-1}$	$4.80*10^{-1}$	$1.867*10^{-1}$
775 °C	$6.48*10^{-5}$	$7.29*10^{-3}$	$2.83*10^{-1}$	$5.19*10^{-1}$	$1.90*10^{-1}$
762.5 °C	$5.225*10^{-5}$	$5.63*10^{-3}$	$2.09*10^{-1}$	$5.89*10^{-1}$	$1.96*10^{-1}$
750 °C	$4.0*10^{-5}$	$4.80*10^{-3}$	$1.68*10^{-1}$	$6.28*10^{-1}$	$2.0*10^{-1}$

Table 8. Temperature distribution of the syngas OK800 and relative species quantities between 800 °C and 750 °C

	$x_{0,CH4}$	$x_{0,H2}$	$x_{0,CO}$	$x_{0,CO2}$	$x_{0,H2O}$
800 °C	$9.806*10^{-5}$	$4.34*10^{-3}$	$3.84*10^{-1}$	$4.29*10^{-1}$	$1.829*10^{-1}$
787.5 °C	$1.06*10^{-4}$	$4.48*10^{-3}$	$3.42*10^{-1}$	$4.68*10^{-1}$	$1.861*10^{-1}$
775 °C	$1.06*10^{-4}$	$4.87*10^{-3}$	$3.08*10^{-1}$	$4.98*10^{-1}$	$1.89*10^{-1}$
762.5 °C	$1.12*10^{-4}$	$4.84*10^{-3}$	$2.42*10^{-1}$	$5.59*10^{-1}$	$1.94*10^{-1}$
750 °C	$1.21*10^{-4}$	$5.23*10^{-3}$	$2.25*10^{-1}$	$5.74*10^{-1}$	$1.95*10^{-1}$

Table 9. Temperature distribution of the syngas OK500 and relative species quantities between 800 °C and 750 °C

The model results show that pre-treatment of biomass at 500 °C is best for the syngas concentrations available for tubular cells. Pre-treatment at 500 °C leads to a good yield in terms of CO concentration (38.4%) while a slight decrease in H_2 is less relevant (0.43%). Similar results are achieved by Guizani et al. (2014) [50].

2D model reconstruction

The main objective is to recreate a syngas-powered stack for the production, under nominal conditions, of 200 W; i.e. 8 W per cell.

First of all, it was necessary to verify the consistency of the dimensionless electrodes hypothesis by reconstructing the 2D model of a single cell, fed by biomass pre-treated at 800 °C, without volumetric electrodes and comparing the results with those obtained by Somano et al. (2021) [29]. The resulting difference is due to some cold spots in the temperature distribution within the model. The model is finished using volumetric electrodes. The thickness of the anodic/cathodic GDL amount to $1.95*10^{-5}$ m and the anodic/cathodic catalyst layer has got a thickness of $1.05*10^{-5}$ m, while the tube cell length was fixed to 16 cm. The power goal is achieved with the scaled-down model with an electrical power output of 8.66 W. The polarization curves (i-V and i-p) of the 2D model are reported below:

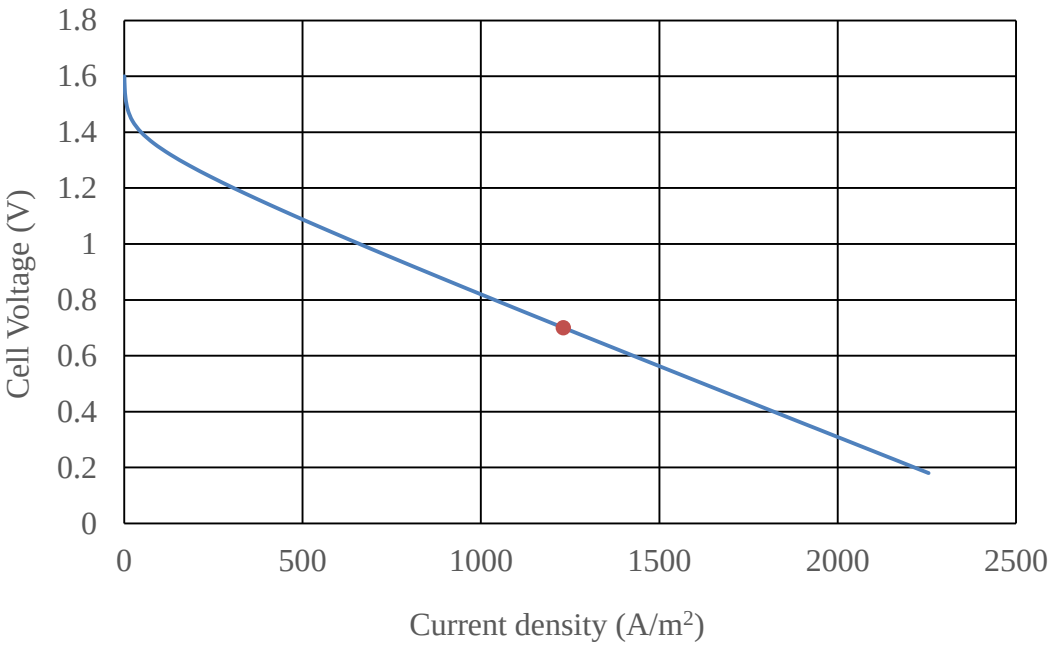

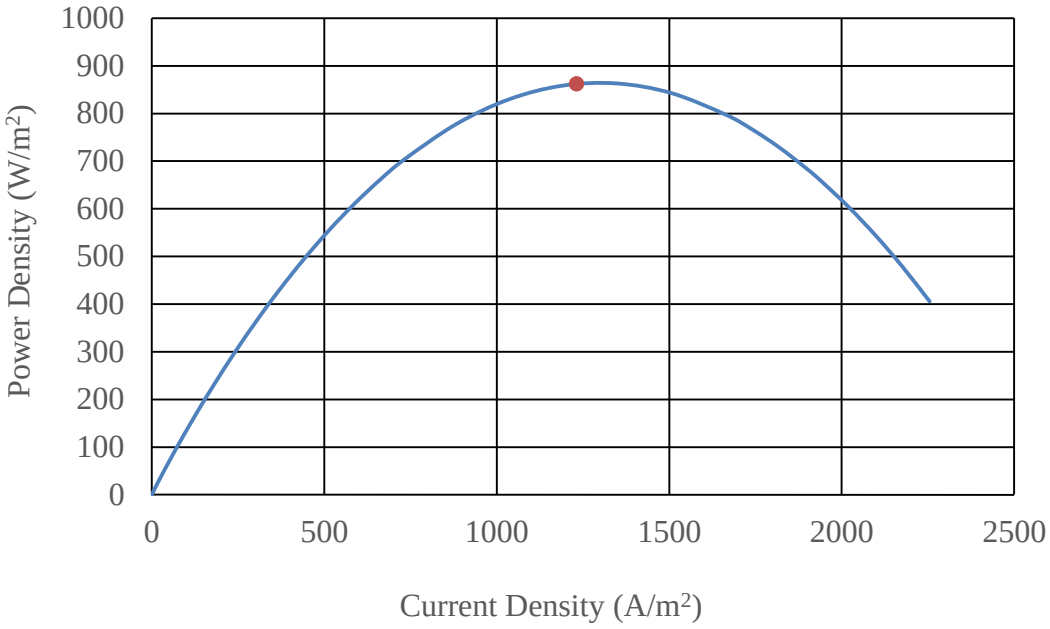

Figure 3. Polarization curves of the tubular cell 2D model

A similar model was approached by Kattke et al. (2011) where a tubular cell powered by liquid fuels is investigated [51]. The 1-D CFD electrochemical model shows a cell electrical power ranging from 7.6 to 10.8 W.

3D model

Afterwards, the same cell shown above was modelled using a 3D model with a coarser mesh to limit the computational cost. In this 3D model, the material properties were taken into account by including their dependence on the temperature distribution achieved. The maximum electrical power achieved by a single tubular cell is 9.5 W. Adding into the model the temperature control system, the temperature distribution improves. The electrical output increases with both water and air temperature control. As can be seen from the figure below (Fig. 4), the tubular cell has a higher level and a more uniform Temperature distribution with the air system and the electrical power goes up to 12.63 W (see Table 10).

	Water cooling system	**Air cooling system**
Electrical current (A)	16.52	18.05

Electrical power (W)	11.57	12.63
Efficiency (%)	27.18	29.68
AU (%)	51.57	56.32
FU (%)	56.8	62.0
Conversion efficiency (%)	47.85	47.85

Table 10. Overall results of the 3D model with the two different cooling systems

The difference in power output is due to the inhibition of the upper part of the cell by the water cooling system, because, due to the enormous difference between the temperature inside the cell and the temperature of the fluid, the ionic conductivity of the electrolyte in this area reaches a value close to zero. The conversion efficiency of the syngas within the electrochemical reaction is constant. The parameter penalised by the water temperature control system is the overall efficiency of the cell, which in turn is linked to the limitations induced on the electric current and consequently on the electric power. Consequently, the cell FU also decreases.

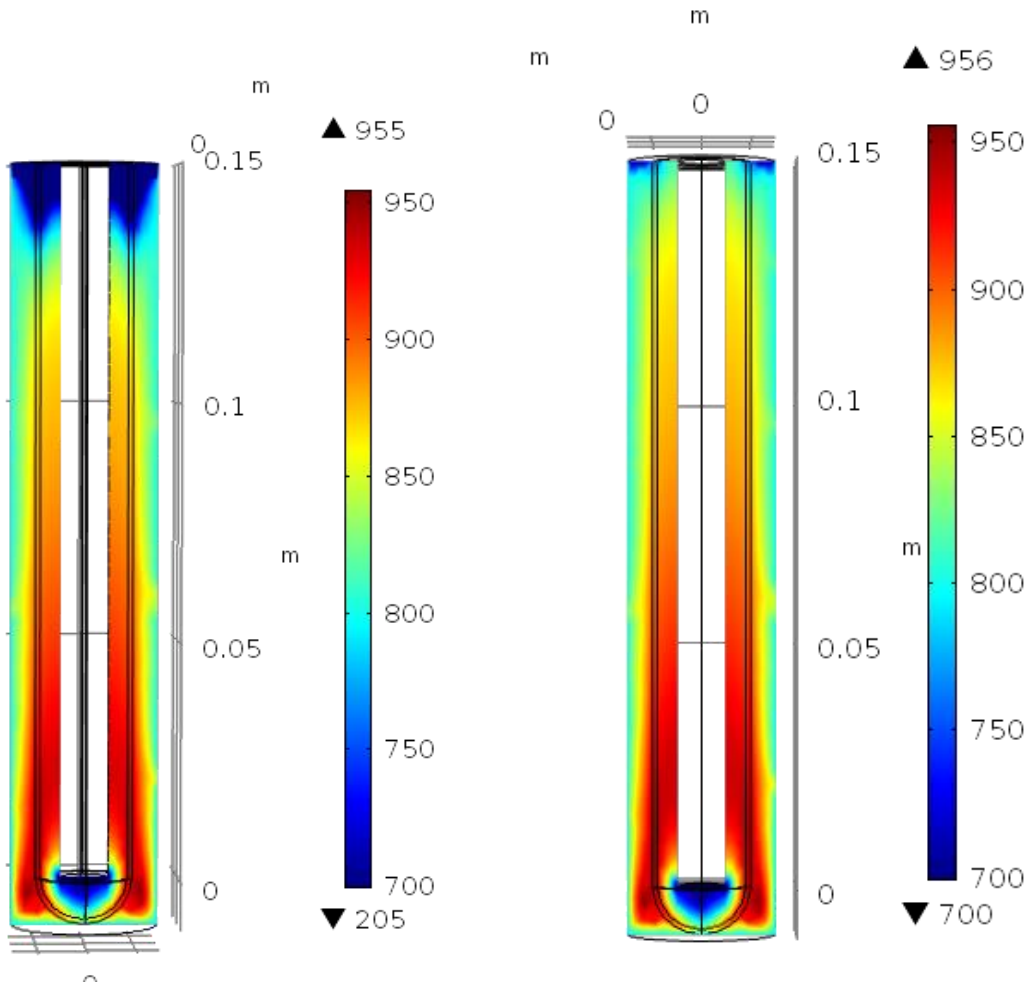

Figure 4. Temperature distribution inside a 3D cell cooled by water (on the left) and cooled by air (on the right)

As reported by Boigues-Munoz et al. (2014), the temperature control is of great importance in the system overall efficiency [52].

This manuscript focuses on the arrangement study of the individual tubular cells for the 200 W SOFC stack. The arrangement of the tubular cells is carried out either as a square (32 cm side) or in a circle configuration (36.3 cm). The aim is to choose the best temperature control system for the two cell arrangements. The molar composition of syngas from residual biomass is defined in the initial part of the chapter. The arrangement of the cells in a square or circle is shown in the following figure 5.

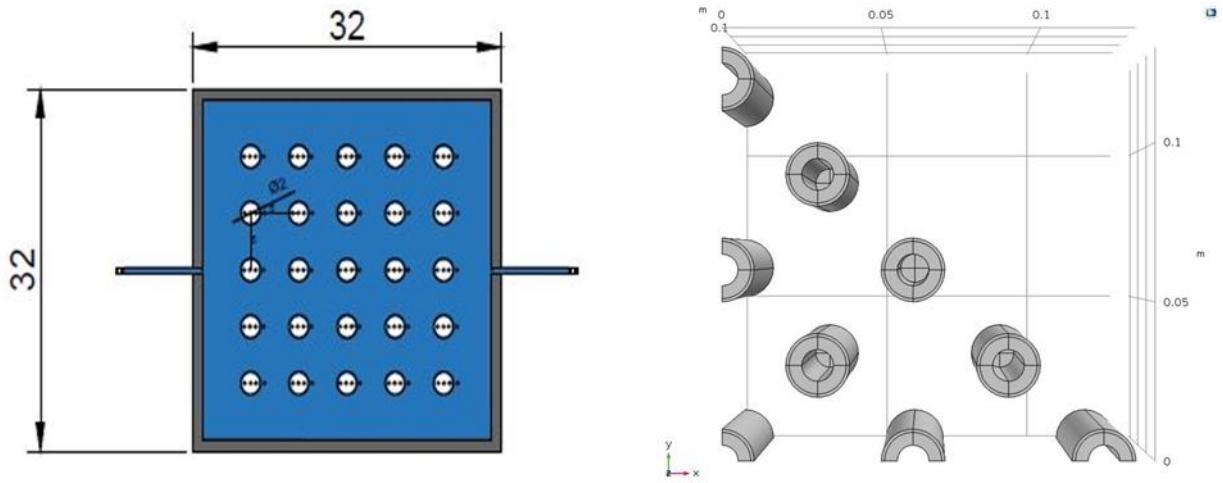

Figure 5. The two stacks configurations - on the left the square configuration and on the right the circular configuration

The connections between the cells are established by connectors outside the stack at the top of the tubular cells. There is no influence of the connectors within the fluidic current of the syngas. Cells in square configuration are connected in series. The connection features of the tubular cells in circular configuration is reported below:

- connect the 5 cells in position 0 m in series;
- connect 4 cells in position -0.03 m with 1 cell in position -0.06 m and, symmetrically, the correspective cells on the right of the stack;
- connect the last 10 cells, five by five, on the right and on the left of the stack.

The electrical powers produced by the stack in circular or square configuration are shown in the following tables. The dependence of the power production on the operating temperature variation is also shown. The selected range starts at 650 °C and goes up to 800 °C.

Power Outputs – Squared Stack

	Water cooling	**Air cooling**
800 – 750 °C	206 W	219 W

800 – 700 °C	162 W	171 W
800 – 650 °C	135 W	142 W

Table 11. Power outputs of the squared stack powered by the 800 °C pre-treated biomass

Power Outputs – Circular Stack

	Water cooling	**Air cooling**
800 – 750 °C	193 W	204 W
800 – 700 °C	136 W	141 W
800 – 650 °C	104 W	106 W

Table 12. Power outputs of the circular stack powered by the 800 °C pre-treated biomass

The tables show how the electrical power produced by the SOFC tubular cell stack with air temperature control is advantageous, under all conditions, compared to temperature control with pressurised water. The electrical power produced with a temperature distribution of 50 °C is advantageous and allows to achieve the target electrical power of 200 W. The best configuration is the square configuration for all temperature conditions and stack temperature control system. This result is due to the better and more uniform temperature distribution under the same operating conditions. The electrical power distribution within the stack is presented in figure 6 (squadre configuration 5x5 cells). The best temperature control system has been chosen, while the role of the pre-treatment temperature is highlighted (500 °C and 800 °C).

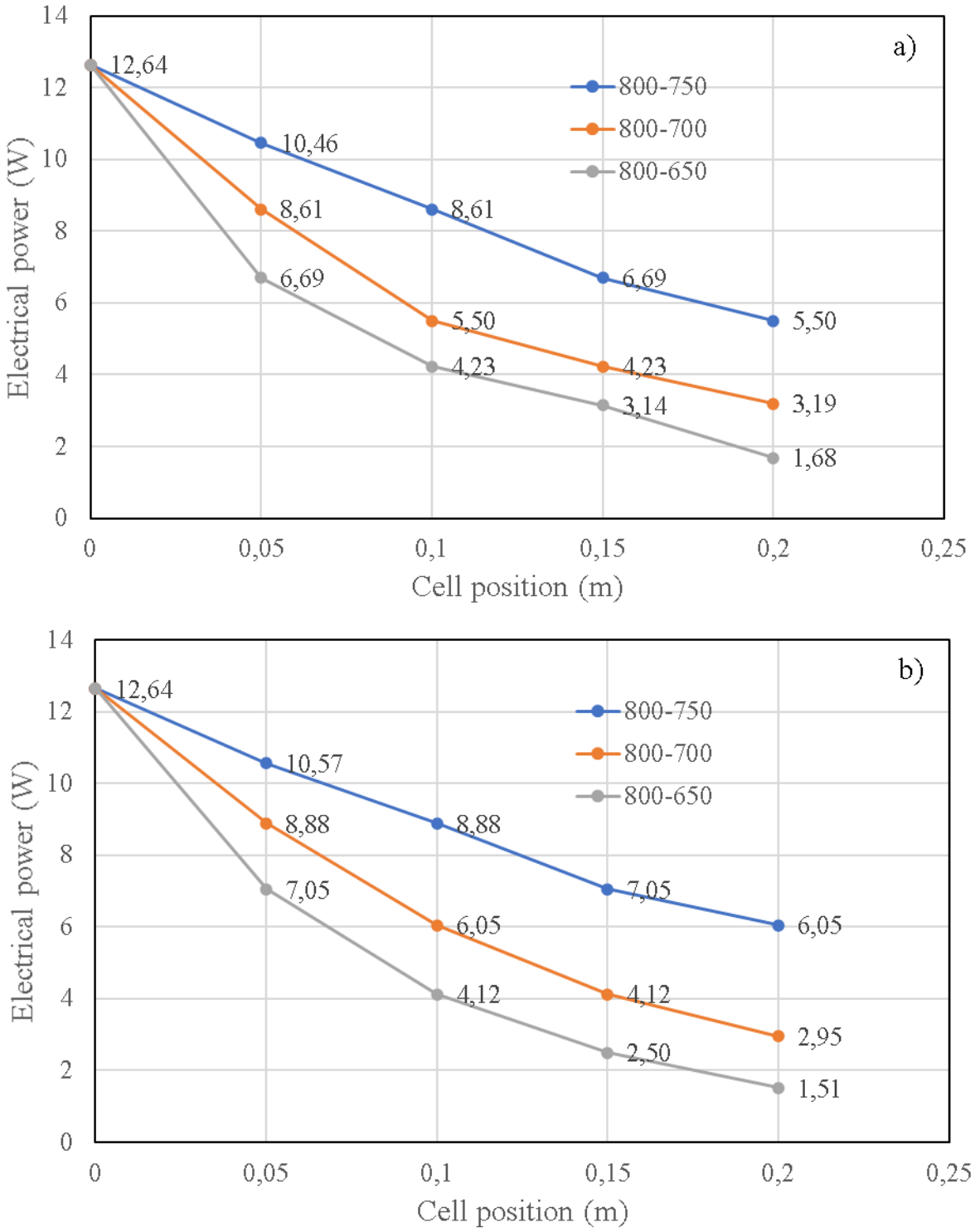

Figure 6. Electrical power distribution in the stack – a) biomass pre-treated at 800 °C and b) at 500 °C

The tubular cells arranged 5x5 in each position, from position 0 to 0.2 m, are able to provide 219 W with biomass pre-treated at 800 °C, while provide 225 W with biomass pre-treated at 500 °C. The results achieved by the model show better results for cells arranged in a square configuration, operating with the biomass pre-treated at 500 °C and controlled with air.

5. Conclusions

The SOFC tubular cell system fed directly by residual biomass from the Mediterranean areas was investigated. The study did not concern only the single cell, as done in the previous publication, but involved several aspects. The focus was on the syngas mixture obtained from the biomass, investigating the pre-treatment temperature, the cell layout and the temperature control system of the stack.

In conclusion, the configuration analysis showed that the best solution in terms of extracted power will be the square stack fed by the biomass pre-treated at 500 °C. The maximum electrical power output is achieved for the square tubular cell configuration, reaching 225 W. This power is distributed in the 5 by 5 rows of tubular cells controlled by the air system, with an even cell temperature distribution varying between 800 °C and 750 °C. However, with the OK500 pre-treated biomass, a pre-heating chamber will have to be designed to heat the solid fuel in an inert atmosphere, in order to limit the decreasing of CO and H_2. Results of the coupling between the biomass feeding system and the gasification process will be published soon. The biomass feeding system operating at the cell temperature (800 °C) is able to produce 219 W. More generally, it appears that the circular configuration provides less power than the square configuration. The circular configuration is limited by the multiple series connection to the lowest current value. From a thermal point of view, the cells are subjected to high temperatures, especially on the lower part of the stack. Here the cooling system to control the thermal distribution can not operate efficiently. The high temperatures could be an advantage for the endothermic biomass gasification process. The minimum temperature values recorded from the water cooling system are dangerous for the cells integrity. Future works will be required for the carbon deposition phenomena investigation.

Acknowledgements

This work has been partly funded by the European Union under the DB-SOFC project (ERANETMED2-72-246).

Reference

[1] C.A. Díaz González, L. Pacheco Sandoval, Sustainability aspects of biomass gasification systems for small power generation, Renewable and Sustainable Energy Reviews. 134 (2020) 110180. https://doi.org/10.1016/j.rser.2020.110180.

[2] E. Alakangas, M. Junginger, J. van Dam, J. Hinge, J. Keränen, O. Olsson, C. Porsö, A. Martikainen, J. Rathbauer, L. Sulzbacher, P. Vesterinen, J. Vinterbäck, EUBIONET III—Solutions to biomass trade and market barriers, Renewable and Sustainable Energy Reviews. 16 (2012) 4277–4290. https://doi.org/10.1016/j.rser.2012.03.051.

[3] S.K. Sansaniwal, M.A. Rosen, S.K. Tyagi, Global challenges in the sustainable development of biomass gasification: An overview, Renewable and Sustainable Energy Reviews. 80 (2017) 23–43. https://doi.org/10.1016/j.rser.2017.05.215.

[4] D. Ghosh, A. D Sagar, V.V.N. Kishore, Scaling up biomass gasifier use: an application-specific approach, Energy Policy. 34 (2006) 1566–1582. https://doi.org/10.1016/j.enpol.2004.11.014.

[5] A. Ghannadzadeh, A.H. Tarighaleslami, Environmental life cycle assessment of glycerine production: Energy transition from natural gas to biomass, Sustainable Energy Technologies and Assessments. 42 (2020) 100775. https://doi.org/10.1016/j.seta.2020.100775.

[6] S. Potrč, L. Čuček, M. Martin, Z. Kravanja, Sustainable renewable energy supply networks optimization – The gradual transition to a renewable energy system within the European Union by 2050, Renewable and Sustainable Energy Reviews. 146 (2021) 111186. https://doi.org/10.1016/j.rser.2021.111186.

[7] N. Radenahmad, A.T. Azad, M. Saghir, J. Taweekun, M.S.A. Bakar, M.S. Reza, A.K. Azad, A review on biomass derived syngas for SOFC based combined heat and power application, Renewable and Sustainable Energy Reviews. 119 (2020) 109560. https://doi.org/10.1016/j.rser.2019.109560.

[8] D. Papurello, A. Lanzini, L. Tognana, S. Silvestri, M. Santarelli, Waste to energy: Exploitation of biogas from organic waste in a 500 Wel solid oxide fuel cell (SOFC) stack, Energy. 85 (2015) 145–158. https://doi.org/10.1016/j.energy.2015.03.093.

[9] V.M. Soltero, L. Román, M.E. Peralta, R. Chacartegui, Sustainable biomass pellets using trunk wood from olive groves at the end of their life cycle, Energy Reports. 6 (2020) 2627–2640. https://doi.org/10.1016/j.egyr.2020.09.017.

[10] B. Velázquez-Martí, E. Fernández-González, I. López-Cortés, D.M. Salazar-Hernández, Quantification of the residual biomass obtained from pruning of trees in Mediterranean olive groves, Biomass and Bioenergy. 35 (2011) 3208–3217. https://doi.org/10.1016/j.biombioe.2011.04.042.

[11] B. Velázquez-Martí, E. Fernández-González, I. López-Cortés, D.M. Salazar-Hernández, Quantification of the residual biomass obtained from pruning of vineyards in Mediterranean area, Biomass and Bioenergy. 35 (2011) 3453–3464. https://doi.org/10.1016/j.biombioe.2011.04.009.

[12] A. Zabaniotou, Agro-residues implication in decentralized CHP production through a thermochemical conversion system with SOFC, Sustainable Energy Technologies and Assessments. 6 (2014) 34–50. https://doi.org/10.1016/j.seta.2014.01.004.

[13] E. Lorente, M. Millan, N.P. Brandon, Use of gasification syngas in SOFC: Impact of real tar on anode materials, International Journal of Hydrogen Energy. 37 (2012) 7271–7278. https://doi.org/10.1016/j.ijhydene.2011.11.047.

[14] D. Papurello, C. Vitaliano, S. Maisano, A. Lanzini, M. Santarelli, Catalytic stability of a Ni-Catalyst towards biogas reforming in the presence of deactivating trace compounds, Renewable Energy. 127 (2018) 481–494. https://doi.org/10.1016/j.renene.2018.05.006.

[15] D. Papurello, A. Lanzini, P. Leone, M. Santarelli, The effect of heavy tars (toluene and naphthalene) on the electrochemical performance of an anode-supported SOFC running on bio-syngas, Renewable Energy. 99 (2016). https://doi.org/10.1016/j.renene.2016.07.029.

[16] R. Coll, J. Salvadó, X. Farriol, D. Montané, Steam reforming model compounds of biomass gasification tars: Conversion at different operating conditions and tendency towards coke formation, Fuel Processing Technology. 74 (2001) 19–31. https://doi.org/10.1016/S0378-3820(01)00214-4.

[17] D. Papurello, A. Lanzini, S. Fiorilli, F. Smeacetto, R. Singh, M. Santarelli, Sulfur poisoning in Ni-anode solid oxide fuel cells (SOFCs): Deactivation in single cells and a stack, Chemical Engineering Journal. 283 (2016). https://doi.org/10.1016/j.cej.2015.08.091.

[18] A. Hauch, A. Hagen, J. Hjelm, T. Ramos, Sulfur Poisoning of SOFC Anodes: Effect of Overpotential on Long-Term Degradation, Journal of the Electrochemical Society. 161 (2014) F734–F743. https://doi.org/10.1149/2.080406jes.

[19] A. Weber, S. Dierickx, A. Kromp, E. Ivers-Tiffée, Sulfur poisoning of anode-supported SOFCs under reformate operation, Fuel Cells. 13 (2013) 487–493. https://doi.org/10.1002/fuce.201200180.

[20] V. Subotić, C. Schluckner, B. Stoeckl, M. Preininger, V. Lawlor, S. Pofahl, H. Schroettner, C. Hochenauer, Towards practicable methods for carbon removal from Ni-YSZ anodes and restoring the performance of commercial-sized ASC-SOFCs after carbon deposition induced degradation, Energy Conversion and Management. 178 (2018) 343–354. https://doi.org/10.1016/j.enconman.2018.10.022.

[21] C. Schluckner, V. Suboti, V. Lawlor, C. Hochenauer, Three-dimensional numerical and experimental investigation of an industrial-sized SOFC fueled by diesel reformat e Part I : Creation of a base model for further carbon deposition modeling, Journal of Hydrogen Energy. 39 (2014) 19102–19118. https://doi.org/10.1016/j.ijhydene.2014.09.108.

[22] M. Cimenti, J.M. Hill, Thermodynamic analysis of solid oxide fuel cells operated with methanol and ethanol under direct utilization, steam reforming, dry reforming or partial oxidation conditions, Journal of Power Sources. 186 (2009) 377–384. https://doi.org/10.1016/j.jpowsour.2008.10.043.

[23] E. Pieratti, M. Baratieri, S. Ceschini, L. Tognana, P. Baggio, Syngas suitability for solid oxide fuel cells applications produced via biomass steam gasification process: Experimental and modeling analysis, Journal of Power Sources. 196 (2011) 10038–10049. https://doi.org/10.1016/j.jpowsour.2011.07.090.

[24] D. Papurello, L. Tomasi, S. Silvestri, M. Santarelli, Evaluation of the Wheeler-Jonas parameters for biogas trace compounds removal with activated carbons, Fuel Processing Technology. 152 (2016) 93–101. https://doi.org/10.1016/j.fuproc.2016.06.006.

[25] D. Papurello, L. Tomasi, S. Silvestri, Proton transfer reaction mass spectrometry for the gas cleaning using commercial and waste-derived materials: focus on the siloxane removal for SOFC applications, International Journal of Mass Spectrometry. (2018). https://doi.org/10.1016/j.ijms.2018.05.002.

[26] D. Papurello, Direct injection mass spectrometry technique for the odorant losses at ppb(v) level from nalophan™ sampling bags, International Journal of Mass Spectrometry. 436 (2019) 137–146. https://doi.org/10.1016/j.ijms.2018.12.008.

[27] R.Ø. Gadsbøll, A. Vivar Garcia, J. Ahrenfeldt, U.B. Henriksen, Solid oxide fuel cell stack coupled with an oxygen-blown TwoStage gasifier using minimal gas cleaning, Renewable Energy. 139 (2019) 1255–1262. https://doi.org/10.1016/j.renene.2019.03.038.

[28] P.V. Aravind, W. De Jong, Evaluation of high temperature gas cleaning options for biomass gasification product gas for Solid Oxide Fuel Cells, Progress in Energy and Combustion Science. 38 (2012) 737–764. https://doi.org/10.1016/j.pecs.2012.03.006.

[29] V. Somano, D. Ferrero, M. Santarelli, D. Papurello, CFD model for tubular SOFC directly fed by biomass, International Journal of Hydrogen Energy. 46 (2021) 17421–17434. https://doi.org/10.1016/j.ijhydene.2021.02.147.

[30] M. Andersson, J. Yuan, B. Sundén, SOFC modeling considering electrochemical reactions at the active three phase boundaries, International Journal of Heat and Mass Transfer. 55 (2012) 773–788. https://doi.org/10.1016/j.ijheatmasstransfer.2011.10.032.
[31] B. Kenney, M. Valdmanis, C. Baker, J.G. Pharoah, K. Karan, Computation of TPB length, surface area and pore size from numerical reconstruction of composite solid oxide fuel cell electrodes, Journal of Power Sources. 189 (2009) 1051–1059. https://doi.org/10.1016/j.jpowsour.2008.12.145.
[32] D. Papurello, S. Silvestri, S. Modena, Biogas trace compounds impact on high-temperature fuel cells short stack performance, International Journal of Hydrogen Energy. 46 (2021) 8792–8801. https://doi.org/10.1016/j.ijhydene.2020.11.273.
[33] S. Park, J. Hyun, C. Jeong, C. Woong, R. Song, J. Lee, Ni-YSZ-supported tubular solid oxide fuel cells with GDC interlayer between YSZ electrolyte and LSCF cathode, International Journal of Hydrogen Energy. 39 (2014) 12894–12903. https://doi.org/10.1016/j.ijhydene.2014.06.103.
[34] K. Chen, L. Zhang, M. Gholizadeh, N. Ai, M.M. Hasan, D. Mourant, C.-Z. Li, S.P. Jiang, Feasibility of tubular solid oxide fuel cells directly running on liquid biofuels, Chemical Engineering Science. 154 (2016) 108–118. https://doi.org/10.1016/j.ces.2016.04.024.
[35] K. Sato, M. Naito, H. Abe, Electrochemical and mechanical properties of solid oxide fuel cell Ni/YSZ anode fabricated from NiO/YSZ composite powder, J. Ceram. Soc. Japan. 119 (2011) 876–883. https://doi.org/10.2109/jcersj2.119.876.
[36] D. Cui, L. Liu, Y. Dong, M. Cheng, Comparison of different current collecting modes of anode supported micro-tubular SOFC through mathematical modeling, Journal of Power Sources. 174 (2007) 246–254. https://doi.org/10.1016/j.jpowsour.2007.08.094.
[37] M. Ni, Modeling of SOFC running on partially pre-reformed gas mixture, International Journal of Hydrogen Energy. 37 (2012) 1731–1745. https://doi.org/10.1016/j.ijhydene.2011.10.042.
[38] M. Santarelli, P. Leone, M. Calì, G. Orsello, Experimental evaluation of the sensitivity to fuel utilization and air management on a 100 kW SOFC system, Journal of Power Sources. 171 (2007) 155–168. https://doi.org/10.1016/j.jpowsour.2006.12.032.
[39] S.P. Jiang, Development of lanthanum strontium manganite perovskite cathode materials of solid oxide fuel cells: A review, 2008. https://doi.org/10.1007/s10853-008-2966-6.
[40] R.C. Buchanan, S. Pope, Optical and Electrical Properties of Yttria Stabilized Zirconia Crystals, (n.d.).
[41] M. Andersson, J. Yuan, B. Sundén, SOFC modeling considering electrochemical reactions at the active three phase boundaries, International Journal of Heat and Mass Transfer. 55 (2012) 773–788. https://doi.org/10.1016/j.ijheatmasstransfer.2011.10.032.
[42] V. Somano, CFD model for tubular SOFC fed directly by biomass, (2019).
[43] M. Ni, 2D heat and mass transfer modeling of methane steam reforming for hydrogen production in a compact reformer, Energy Conversion and Management. 65 (2013) 155–163. https://doi.org/10.1016/j.enconman.2012.07.017.
[44] M. Ceriani, Analisi di modello di SOFC alimentate con gas di sintesi, (2015) 1633.
[45] R.C. Reid, T.K. Sherwood, R.E. Street, The Properties of Gases and Liquids , 2009. https://doi.org/10.1063/1.3060771.
[46] B.A. Haberman, J.B. Young, Three-dimensional simulation of chemically reacting gas flows in the porous support structure of an integrated-planar solid oxide fuel cell, International Journal of Heat and Mass Transfer. 47 (2004) 3617–3629. https://doi.org/10.1016/j.ijheatmasstransfer.2004.04.010.
[47] W. Lehnert, J. Meusinger, F. Thom, Modelling of gas transport phenomena in SOFC anodes, Journal of Power Sources. 87 (2000) 57–63. https://doi.org/10.1016/S0378-7753(99)00356-0.
[48] T. Allison, JANAF Thermochemical Tables, NIST Standard Reference Database 13, (1996). https://doi.org/10.18434/T42S31.
[49] A. Lampropoulos, N. Kaklidis, C. Athanasiou, M.A. Montes-Morán, A. Arenillas, J.A. Menéndez, V.D. Binas, M. Konsolakis, G.E. Marnellos, Effect of Olive Kernel thermal treatment (torrefaction vs. slow pyrolysis) on the physicochemical characteristics and the CO2 or H2O gasification performance of as-prepared biochars, International Journal of Hydrogen Energy. (2020) S0360319920344815. https://doi.org/10.1016/j.ijhydene.2020.11.230.

[50] C. Guizani, Effects of CO2 on the biomass pyro-gasification in High Heating Rate and Low Heating Rate conditions, (n.d.) 277.
[51] K.J. Kattke, R.J. Braun, A.M. Colclasure, G. Goldin, High-fidelity stack and system modeling for tubular solid oxide fuel cell system design and thermal management, Journal of Power Sources. 196 (2011) 3790–3802. https://doi.org/10.1016/j.jpowsour.2010.12.070.
[52] C. Boigues-Muñoz, G. Santori, S. McPhail, F. Polonara, Thermochemical model and experimental validation of a tubular SOFC cell comprised in a 1 kW el stack designed for µCHP applications, International Journal of Hydrogen Energy. 39 (2014) 21714–21723. https://doi.org/10.1016/j.ijhydene.2014.09.021.

Declaration of interests

☒ The authors declare that they have no known competing financial interests or personal relationships that could have appeared to influence the work reported in this paper.

☐The authors declare the following financial interests/personal relationships which may be considered as potential competing interests:

Declarations of interest: none